The Astrophysical Journal, 926:94 (8pp), 2022 February 10 https://doi.org/10.3847/1538-4357/ac46c8

Cosmic-ray Transport in Magnetohydrodynamic Turbulence

Snehanshu Maiti[1,2], Kirit Makwana[3], Heshou Zhang[2,1], and Huirong Yan[1,2]
[1] Deutsches Elektronen-Synchrotron DESY Platanenalle 6, D-15738 Zeuthen, Germany; huirong.yan@desy.de
[2] Institute fur Physik und Astronomie Universitat Potsdam, Haus 28, Karl-Liebknecht-Str 24/25,D-14476 Potsdam, Germany
[3] Department of Physics, Indian Institute of Technology Hyderabad Medak, Telangana 502285, India
Received 2021 August 3; revised 2021 December 20; accepted 2021 December 20; published 2022 February 16

Abstract

This paper studies cosmic-ray (CR) transport in magnetohydrodynamic (MHD) turbulence. CR transport is strongly dependent on the properties of the magnetic turbulence. We perform test particle simulations to study the interactions of CR with both total MHD turbulence and decomposed MHD modes. The spatial diffusion coefficients and the pitch angle scattering diffusion coefficients are calculated from the test particle trajectories in turbulence. Our results confirm that the fast modes dominate the CR propagation, whereas Alfvén and slow modes are much less efficient and have shown similar pitch-angle scattering rates. We investigate the cross field transport on large and small scales. On large/global scales, normal diffusion is observed and the diffusion coefficient is suppressed by M_A^{ζ} compared to the parallel diffusion coefficients, with ζ closer to 4 in Alfvén modes than that in total turbulence, as theoretically expected. For the CR transport on scales smaller than the turbulence injection scale, both the local and global magnetic reference frames are adopted. Superdiffusion is observed on such small scales in all the cases. Particularly, CR transport in Alfvén modes show clear Richardson diffusion in the *local* reference frame. The diffusion transitions smoothly from the Richardson's one with index 1.5 to normal diffusion as the particle mean free path decreases from $\lambda_{\parallel} \gg L$ to $\lambda_{\parallel} \ll L$, where L is the injection/coherence length of turbulence. Our results have broad applications to CRs in various astrophysical environments.

Unified Astronomy Thesaurus concepts: Cosmic rays (329); Particle astrophysics (96); Magnetohydrodynamics (1964); Plasma astrophysics (1261); Magnetohydrodynamical simulations (1966); Magnetic fields (994)

1. Introduction

Magnetohydrodynamic (MHD) turbulence is ubiquitous in astrophysical plasmas ranging from the interplanetary space to the interstellar and intergalactic medium. The propagation of cosmic rays (CRs) is determined by their interactions with the magnetic turbulence. Unlike hydrodynamic turbulence, MHD turbulence can be decomposed into three plasma modes: Alfvénic modes, and magnetosonic slow and fast modes (Cho & Lazarian 2002). The Alfvén and slow modes have shown scale-dependent anisotropy (Goldreich & Sridhar 1995; Lithwick & Goldreich 2001), whereas fast modes are much more isotropic (Cho & Lazarian 2003; Makwana & Yan 2020). The scattering of CRs can be characterized by their interaction with the three MHD modes (see, e.g., Schlickeiser 2002). Because of the anisotropy of Alfvénic turbulence, the cosmic-ray scattering and acceleration in turbulence has been demonstrated to be dominated by compressible MHD modes, particularly the isotropic fast modes (Yan & Lazarian 2002, 2004, 2008; Yan et al. 2008). CR transport, therefore, depends much on the MHD modes composition of turbulence, which varies depending mostly on the driving mechanism of MHD turbulence (Makwana & Yan 2020).

The cross field transport is also shown to differ in the tested model of turbulence than from earlier scenarios. A popular concept before was that CR undergoes subdiffusion owing to field line random walk (see, e.g., Kóta & Jokipii 2000). Observations of solar energetic particles in the heliosphere indicated a faster diffusion process perpendicular to the solar magnetic field. The magnetic field separation in Alfvénic turbulence presents a close analog of the separation of particles in turbulent media due to the well-known process of Richardson diffusion (Richardson 1926; Lazarian et al. 2004; Maron et al. 2004). It is demonstrated that subdiffusion does not apply and instead CR cross field transport is diffusive on large scales and superdiffusive on small scales (Yan & Lazarian 2008). Superdiffusion has also been observed in both the solar wind (Perri & Zimbardo 2009) and supernova remnants in the interstellar medium (Perri et al. 2016).

Because of the nonlinear nature of turbulence, it is necessary to test the theories with numerical simulations. Earlier numerical simulations employed only total MHD turbulence and the global magnetic field as reference (Beresnyak et al. 2011; Xu & Yan 2013). We conduct systematic studies of particle transport in this paper, comparing the contributions from total MHD turbulence as well as those from individual MHD modes. The latter is crucial as proportion can vary in real astrophysical environments (Zhang et al. 2020), and this can be a key factor in determining the local diffusion coefficient, which can substantially deviate from the Galactic mean value (see, e.g., Abeysekara et al. 2017). We also adopt reference frames defined by both the global and local magnetic magnetic fields as they generally differ in turbulence environments. The CR transport in the local reference frame is essential for the study of particle transport on small scales, e.g., near sources where CRs are freshly injected (e.g., Liu et al. 2019). Also, unlike earlier studies, we focus on particles of Larmor radii within the inertial range so that the test particle simulation results can be directly confronted with the theoretical results.

In this paper, we perform test particle simulations in Section 2. We investigate how pitch-angle scattering differs among different modes in Section 3. We present the results of

Table 1
Alfvénic Mach Numbers of Turbulence Data Cubes Employed in Our Simulations

M_A for simulations in whole turbulence data						
0.44	0.56	0.65	0.83	1.28	1.40	1.54
M_A for tests in decomposed turbulence data						
0.40	0.50	0.65	0.68	0.73	0.80	0.91

Note. The first row are data cubes only for the test particle simulations with whole turbulence data cubes. The second row are the data cubes with decomposition performed.

perpendicular and parallel diffusion of CRs on global scales in Section 4. The perpendicular transport of CRs on scales smaller than the turbulence injection scale is studied in Section 5. Our results are summarized in Section 6.

2. Numerical Setups

We have performed 3D MHD simulations to generate turbulence data cubes using two types of MHD codes: the one based on Cho & Lazarian (2002); the other with PENCIL codes.[4] The turbulence data cubes are set with $L_{\rm box}^3 = 512^3$ resolution and energy injection scale of $L \sim 0.4 L_{\rm box}$. The 3D turbulences are driven by solenoidal forcing. Upon the full development of MHD turbulence, snapshots of turbulence are employed in the test particle simulations. We modulate the external mean magnetic field to produce MHD turbulence with different Alfvénic Mach number M_A, defined by:

$$M_A \equiv < \frac{\delta V}{V_A} > \sim \frac{\delta B}{B_0}. \quad (1)$$

Here the quantity V_A is the Alfvénic velocity, the symbol "$< ... >$" indicates the spatial average, and δB and B_0 are the turbulent and average magnetic field, respectively. The M_A values of the generated turbulence data cubes are listed in Table 1. We also consider the CR transport in decomposed MHD modes. Based on the method described in Cho & Lazarian (2002, 2003), the 3D MHD turbulence is decomposed into three eigenmodes: Alfvén, slow, and fast. The energy of the magnetic fluctuations for the decomposed modes are normalized to the same amplitude as the total turbulence data cubes. Hence, the decomposed modes and the total turbulence have the same M_A.

Test particle simulations are carried out in the MHD turbulence to trace the trajectories of CRs. Since the relativistic particles considered in our study have speed much larger than the Alfvén speed, the magnetic fields are considered as stationary, and the electric fields in the turbulent plasma are neglected for the study of CR transport. The particle motion is governed by:

$$m\gamma \frac{d\boldsymbol{v}}{dt} = q(\boldsymbol{v} \times B), \quad (2)$$

where q, m, and $\boldsymbol{v}$ represent the charge, mass, and velocity of the particles, respectively. γ is the Lorentz factor, and $\boldsymbol{B}$ is the turbulent magnetic field. The Larmor radius of the particle is $r_L = mc^2\gamma/eB_0$. In the current simulations, the dissipation scale of turbulence is $\lesssim$0.02 cube size. We choose $r_L = 0.04$ so that it well resides within the inertial range. The particle trajectory tracer follows the Bulrisch Stoer method (Press et al. 1986). The periodic boundary conditions are adopted. The CR diffusion coefficients are calculated from the particle trajectory data.

[4] Please see http://pencil-code.nordita.org for details.

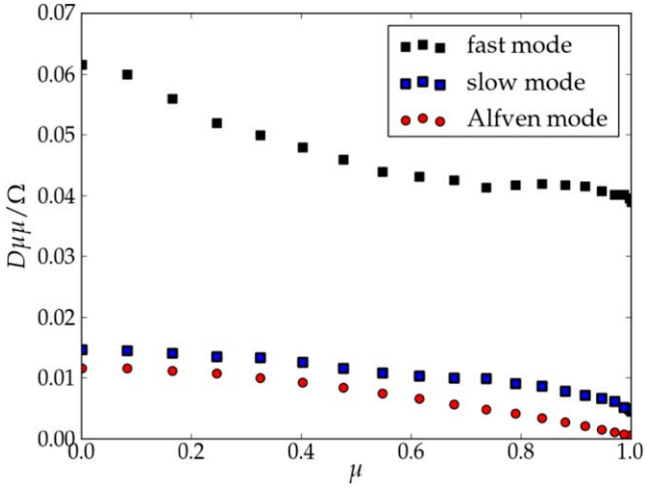

Figure 1. Pitch-angle diffusion coefficients for CRs in different MHD modes with $M_A \sim 0.9$. The x-axis represents the initial pitch-angle cosine, μ. The y-axis represents the pitch-angle scattering coefficient normalized by the gyrofrequency, $D_{\mu\mu}/\Omega$. Different symbols represent different MHD modes: Alfvén (red), slow (blue), and fast (green).

3. Pitch-angle Scattering

CR pitch-angle scattering is studied here by injecting CRs into MHD modes with the same initial pitch angle μ_0 but random initial positions. The initial pitch-angle cosine μ_0 is varied from 0 to 1 with an interval of 0.05. 10,000 particles are used for each test run. The simulations are performed for a few particle gyroperiods so that the pitch-angle deviation is small (i.e., the root mean square deviation of the pitch-angle cosine is between 0.01 and 0.1). The pitch-angle diffusion coefficient is defined by

$$D_{\mu\mu} = \left\langle \frac{(\mu - \mu_0)^2}{2t} \right\rangle, \quad (3)$$

where the result is averaged among the particles.

The pitch-angle diffusion coefficients and their variation with initial pitch angle cosines are presented in Figure 1 for the three MHD modes: Alfvén, slow, and fast. The result agrees well with the prediction of the nonlinear theory in Yan & Lazarian (2008; hereafter YL08). Compressible modes contribute to particle scattering through both gyroresonance and resonant mirror (transit time damping (TTD)) interaction, the latter of which only operates with compressible modes. Alfvén modes, on the other hand, only scatter particles through gyroresonance. This is why slow modes are slightly more efficient in scattering particles despite the fact that they have similar anisotropy as Alfvén modes. In comparison to the anisotropic Alfvén and slow modes, scattering with isotropic fast modes are more efficient. We note that the inertial range in the current MHD simulations is limited. The interstellar turbulence cascade spans more than 10 decades (Armstrong et al. 1995; Chepurnov & Lazarian 2010). CRs experience, therefore, much more anisotropic Alfvénic turbulence on the

Table 2
Mean Free Path $\lambda_{\parallel}$ (in unit of box size) Calculated from $D_{\parallel}$ and $D_{\mu\mu}$

M_A	0.4	0.5	0.65	0.68	0.73	0.8	0.91
$\lambda_{\parallel}$ from $D_{\parallel}$	12.7	10.25	9.3	5.8	3.5	1.92	1.2
$\lambda_{\parallel}$ from $D_{\mu\mu}$	12.5	10.03	9.1	5.9	3.3	1.9	1.15

Note. The mean free paths in the unit of box size obtained are similar in value from both the above methods of calculation.

resonant scales, which are 6–7 orders of magnitude smaller than the turbulence injection scale (∼100 pc) in the interstellar medium. This indicates the role of fast modes in scattering CRs is even more prominent in the Galactic ISM.

The pitch-angle scattering determines the diffusion of CRs parallel to the magnetic field. By inserting $D_{\mu\mu}$ from our simulation into the following equation, the parallel mean free path of CR ($\lambda_{\parallel}$) can be calculated (Earl 1974):

$$\frac{\lambda_{\parallel}}{L} = \frac{3}{4}\int_0^1 \frac{d\mu v(1-\mu^2)^2}{D_{\mu\mu}L}. \quad (4)$$

This calculation will be further cross-checked with the parallel diffusion discussed in the next section.

4. Particle Transport on Large Scales

The CR diffusion is strongly dependent on the transportation scale, i.e., larger or smaller than the magnetic coherence length of the turbulence (at the injection scale L for our simulations). Hence, we will separate the calculations for the two cases and only focus on the large-scale transport in this section.

We set random initial position and random initial pitch angles for CRs with large-scale transport. 2000 particles are used for each simulation. The simulations are run in total turbulence and decomposed MHD modes with different Alfvénic Mach numbers. The simulations are carried out for thousands of particle gyroperiods until a normal diffusion regime is reached (see Figure A1 in the Appendix for details).

In the current simulations, the mean magnetic field is in the x-direction; hence the perpendicular diffusion coefficient ($D_{\perp}$) is calculated as:

$$D_{\perp} = \left\langle \frac{(y-y_0)^2 + (z-z_0)^2}{2t} \right\rangle. \quad (5)$$

The parallel diffusion coefficient ($D_{\parallel}$) is calculated as:

$$D_{\parallel} = \left\langle \frac{(x-x_0)^2}{2t} \right\rangle. \quad (6)$$

The parallel mean free path of particles $\lambda_{\parallel}$ is related to $D_{\parallel}$ by $\lambda_{\parallel} = 3D_{\parallel}/v$. The $\lambda_{\parallel}$ calculated this way is comparable to those obtained from $D_{\mu\mu}$ in Equation (4) and presented in Table 2.

The mean free path in the simulations is large, $\lambda_{\parallel} > L$, due to the limited numerical resolution and therefore limited inertial range. The regime $\lambda_{\parallel} > L$ corresponds to the transport of ultra-high-energy CRs and high-energy Galactic CRs in molecular clouds.

On the other hand, the mean free path for most Galactic CRs is smaller than the energy injection scale ($\lambda_{\parallel} < L$). In order to study this regime, more scatterings are artificially introduced in the test particle simulations. In each time step of particle motion, the pitch-angle scattering is artificially boosted by a constant factor to bring the mean free path below the injection length of turbulence. The higher the boosting factor is, the less is the mean free path obtained for the particles.

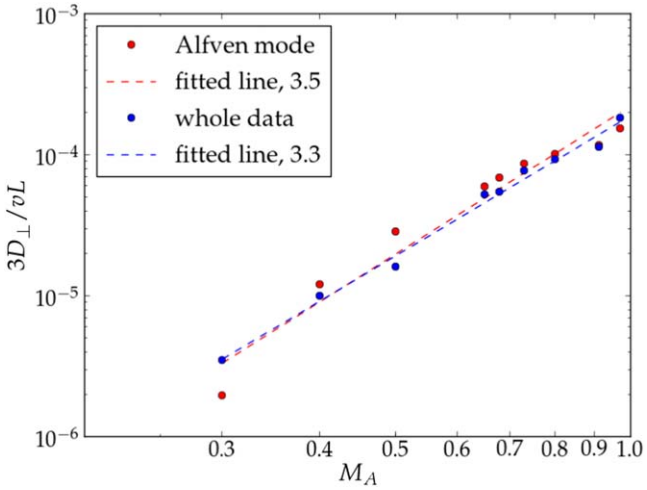

Figure 2. The perpendicular diffusion coefficient with $\lambda_{\parallel} > L$ in MHD turbulence of various M_A. The results are obtained for the Alfvén and the whole turbulence data cubes.

The dependence of the perpendicular diffusion coefficient on the Mach number is presented in Figure 2 for both the total turbulence data cubes and the Alfvén modes. The relation between the diffusion coefficients and Alfvénic Mach numbers is fitted by a power law:$D_{\perp} \propto M_A^{\zeta}$. By taking into account the anisotropy of the Alfvénic turbulence, Yan & Lazarian (2008) demonstrated that the relation between perpendicular diffusion $D_{\perp}$ and M_A should have a power-law index $\zeta = 4$ instead of the $\zeta = 2$ scaling calculated by Kóta & Jokipii (2000). As is demonstrated by Figure 2, the index ζ is 3.5 for Alfvén modes and 3.3 for total turbulence data. Both results are more in favor of the YL08 calculation.

We further consider the CR propagation with a mean free path smaller than the injection scale, which is the case for all Galactic CRs. Simulations are executed with the artificial scattering included as aforementioned. In this regime, it is expected that the ratio between perpendicular and parallel diffusion coefficients ($D_{\perp}/D_{\parallel}$) will follow an M_A^4 dependence (Yan & Lazarian 2008). The dependency of the diffusion coefficients on the Mach number is presented in Figure 3 for $\lambda_{\parallel} < L$. The diffusion coefficients are compared for both the Alfvén modes and the total turbulence. As demonstrated in Figure 3, the fitting index is 3.65 for the total turbulence data cubes and 3.83 for Alfvén modes.

For both regimes where the CR mean free path is larger and smaller than the injection scale, the results from Alfvén modes are closer to the expected index $\zeta = 4$ (YL08) than those from total turbulence data cubes. This is due to the contributions from the magnetosonic modes in the total turbulence data cubes. Our calculations show that the CR perpendicular diffusion on large scales is strongly dependent on the Alfvénic Mach number, and it is essential to consider the anisotropy of MHD turbulence when modeling CR propagation.

5. Perpendicular Transport on Scales Smaller than L and Superdiffusion

In this section, we will discuss the particle transport on small scales within the inertial range. The time evolution for the

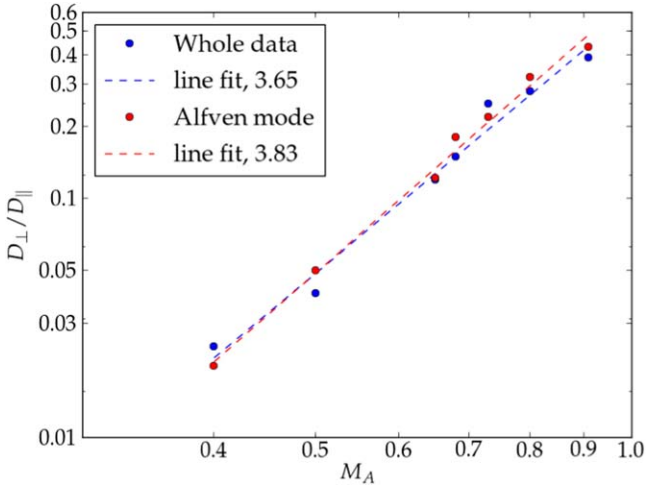

Figure 3. The ratio between perpendicular and parallel diffusion ($D_\perp/D_\parallel$) when $\lambda_\parallel < L$. The transport of particles in both the whole turbulence (blue) and Alfvén modes (red) is presented. The fitting lines and power-law indices are marked in the legend.

perpendicular transport can be fitted by a power law:

$$d_\perp \equiv \langle (y - y_0)^2 + (z - z_0)^2 \rangle^{1/2} \propto t^\alpha. \quad (7)$$

The Richardson diffusion describes the explosive growth of the separation of particles in a turbulence medium, as inferred from fluids experiments many decades ago (Richardson 1926). The Richardson law is equivalent to the Kolmogorov spectrum. Therefore Richardson diffusion is also expected in MHD turbulence because the perpendicular spectrum of Alfvénic turbulence has a Kolmogorov scaling (Goldreich & Sridhar 1995). The Richardson diffusion in MHD turbulence was confirmed with high-resolution numerical simulations by Eyink et al. (2013). Following the Richardson diffusion of magnetic field lines, CRs also undergo superdiffusion on the scales below the injection scale with an index over time of $\alpha = 3/2$ (Yan & Lazarian 2008; Lazarian & Yan 2014).

For the study of CR transport on small scales, test particle simulations are performed in MHD turbulence data cubes with CRs being initially grouped together into beams. The simulation box has 512^3 cells. This box is divided into 64 equally sized cubes of size 128^3 cells. From the center of each of these cubes, a beam is launched parallel to the local magnetic field. The starting points of the beam particles are uniformly distributed around the center of each cube with a separation of 1 cell unit among them. The CRs in each beam are very closely spaced, and their initial pitch angles are set to zero so that it could be analyzed how the particle separation diverges with time. For a particular Mach number, the test particle simulations are done in different MHD modes as well as the total turbulence data cubes. There are two reference frames in the current simulations: the global reference frame, defined by the mean magnetic field of the turbulence data cube, and the local reference frame, defined by the mean magnetic field along the particle trajectory. The evolution of perpendicular CR transport in this work is calculated in both the global and the local frames of reference. The particle position and velocity and the magnetic field at the corresponding position are recorded at each time instance from test particle simulations. The values of the perpendicular distance are obtained by averaging over all combinations of pairs of particles within individual beams and then over all the beams.

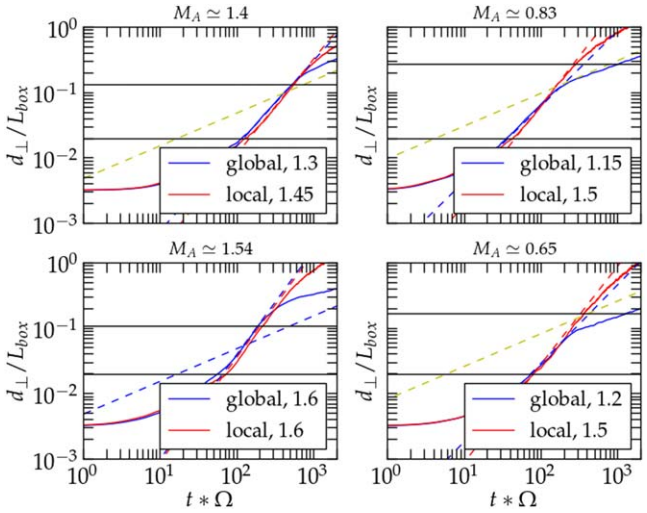

Figure 4. Perpendicular transport of CRs on small scales. The y-axis represents the perpendicular distances normalized by the box length ($d_\perp/L_{box}$), and the x-axis represents the CR gyroperiods ($t * \Omega$). The perpendicular distances obtained from numerical simulations are represented in the global (blue lines) and the local (red lines) reference frames. The horizontal lines in the plots represent the inertial range of turbulence. The yellow lines represent the reference for normal diffusion with a slope of 0.5.

Table 3
The Obtained Superdiffusion Index α

M_A	0.44	0.56	0.65	0.83	1.28	1.4	1.54
Global	0.95	1.1	1.2	1.15	1.25	1.3	1.6
Local	1.3	1.45	1.5	1.5	1.35	1.45	1.7

Note. The diffusion coefficients are calculated and compared in both the global and local frames of reference. CR undergoes superdiffusion, and the slope obtained is closer to 1.5 in the *local* reference frame.

The perpendicular distance $d_\perp$ is plotted against the propagation time of the CRs in Figure 4 for sub-Alfvénic and super-Alfvénic total turbulence data. The results are fitted with Equation (7). Figure 4 demonstrates the CR transport in the two reference frames: all cases can be fitted with an index close to $\alpha \sim 1.5$ in the *local* reference frame, whereas in the global reference frame, α is only close to 1.5 in super-Alfvénic cases, decreasing substantially and becoming close to 1 in sub-Alfvénic cases. In Table 3, the comprehensive fitting indices are listed for the CR superdiffusion in total MHD turbulence data cubes with the Alfvénic Mach number ranging from 0.44 to 1.54. The fitting index is close to Richardson diffusion $\alpha \sim 1.5$ for all data measured in the *local* reference frame, which is in line with the theoretical expectations as the global magnetic field generally differs from local magnetic fields in a turbulent medium. Figure 5 shows the power spectral density (PSD) of the turbulence data and the probability density functions (PDFs) of the test particles launched in the same turbulence data cube versus the distance r between them at different time snapshots. The distribution fits well to an exponential form, i.e., $P \propto \exp(-Cr^{1-h})$; the index $h = 1/3$ is the Kolmogorov scaling, consistent with the Richardson diffusion (Hentschel & Procaccia 1984; Eyink et al. 2013).

We further study the perpendicular transport on small scales from decomposed MHD modes. As an example, Figure 6 demonstrates how we obtain the fitting index for the time evolution of the perpendicular transport in different MHD

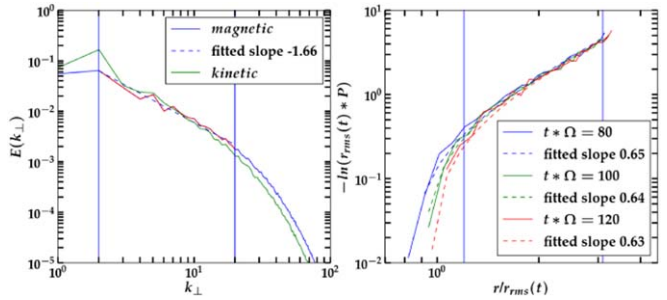

Figure 5. Left: The power spectrum density of turbulence data. Right: The Probability distribution of test particles launched from the same turbulence data cube versus the distance r at given time snapshots. The fitting is consistent with a Kolmogorov spectrum index of $h = 1/3$.

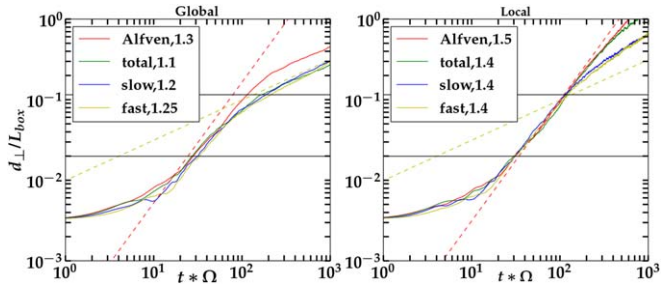

Figure 6. The same as Figure 4 but with $M_A \sim 0.73$, and results for the decomposed modes are included for comparison.

modes. Both the local and global reference frames are used in our calculations. Turbulence data cubes with Alfvénic Mach numbers ranging from 0.4 to 1.0 are considered, and the fitting power-law index α values are presented for the total and decomposed modes in Table 4. Superdiffusion is generally observed in all our tests.[5] From Table 4, we find that the particles in decomposed Alfvénic modes are the closest to the Richardson diffusion (index $\alpha = 1.5$) in the *local* reference frame compared to the other modes. In the global magnetic reference frame, the indices deviate further from the Richardson diffusion, as expected. This implies that the observed diffusion index can vary depending on the modes composition as well as the Alfvénic Mach number of the local turbulence.

We also calculate the M_A dependence of the superdiffusion ${d_\perp}^2/t^3$ of particles. It is expected that for sub-Alfvénic turbulence the dependence is M_A^4, and for super-Alfvénic turbulence the dependence is M_A^3 (Yan & Lazarian 2008; Lazarian & Yan 2014).

Figure 7 demonstrates the CR perpendicular diffusion in Alfvén modes in the sub-Alfvénic regime. The diffusion coefficients are calculated in both the local and global reference frames. The fitting power-law index in the *local* reference frame (4.34) is closer to the theoretical expectation M_A^4 than that in the global frame (4.84).

Figure 8 shows the perpendicular diffusion in super-Alfvénic turbulence for the total data cube and decomposed MHD modes. The inertial range of MHD turbulence starts from LM_A^{-3}. The MHD mode decomposition is only performed within the inertial range. We fit the time evolution of perpendicular transport with Equation (7) when the particles are within the inertial range (indicated by the black lines). The

[5] We randomly selected a few cases to repeat the test particle simulations in higher-resolution turbulence data (1024^3) with the same M_A. The results do not show obvious differences.

Table 4
The Same as Table 3 but the Comparison Extends to Decomposed MHD Modes

M_A	0.4	0.5	0.65	0.68	0.73	0.8	0.91	0.97
Global MM	0.8	1.0	1.1	1.1	1.1	1.2	1.15	1.15
Global AM	1.1	1.65	1.3	1.3	1.3	1.35	1.3	1.4
Global SM	0.95	1.3	1.3	1.1	1.2	1.3	1.2	1.3
Global FM	1.1	1.2	1.1	0.9	1.25	1.25	1.6	1.4
Local MM	1.2	1.5	1.6	1.4	1.4	1.5	1.4	1.4
Local AM	**1.5**	**1.5**	**1.5**	**1.5**	**1.5**	**1.5**	**1.5**	**1.6**
Local SM	1.6	1.4	1.3	1.3	1.4	1.4	1.3	1.3
Local FM	1.55	1.7	1.1	1.3	1.4	1.4	1.7	1.4

Note. AM represents the Alfvén mode, SM represents the slow modes, FM represents the fast mode, and MM represents the total data cube. "Global" and "Local" denote the magnetic reference frames in the calculation.

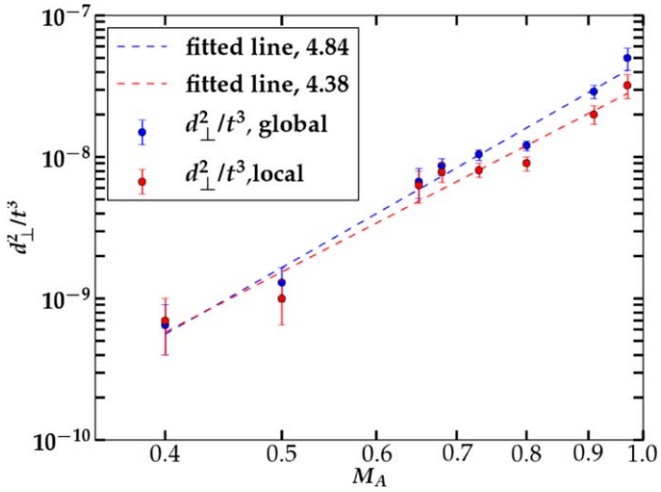

Figure 7. Superdiffusion of particles with $\lambda_\parallel > L$ in Alfvén modes. The blue line is the fit in the global reference frame. The red line shows the fit for the data points obtained in the local reference frame.

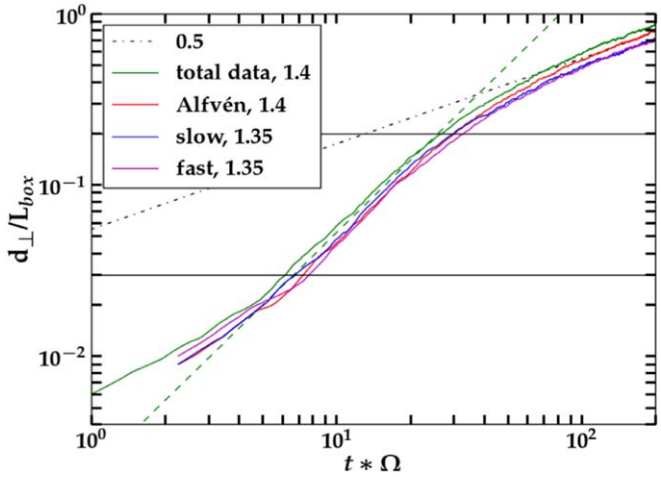

Figure 8. The same as Figure 6 but in the local reference frame with super-Alfvénic turbulence $M_A = 2.11$.

CRs in the decomposed Alfvén modes show superdiffusion with a power-law index of 1.5. The contributions from the magnetosonic modes result in a slightly different power-law index obtained in the total turbulence data (1.4).

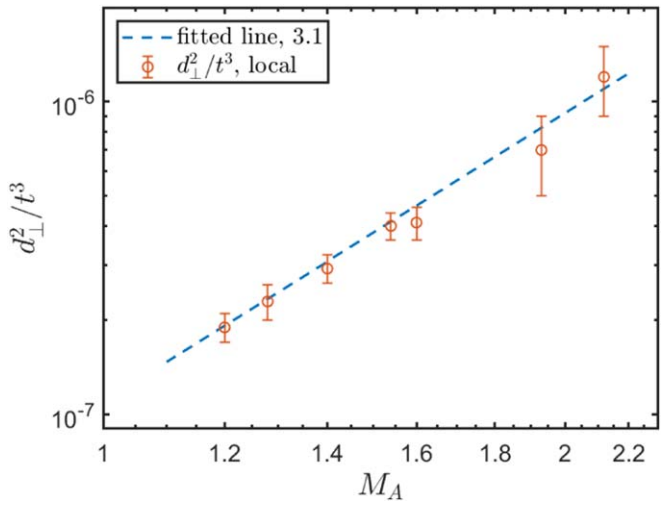

Figure 9. The same as Figure 7 but with super-Alfvénic turbulence. The calculation is done in the local reference frame.

Figure 9 represents the M_A dependence of the perpendicular diffusion at the *local* reference frame in different super-Alfvénic turbulence conditions. The superdiffusion on small scales ${d_\perp}^2/t^3$ in the *local* reference frame show a dependence of $M_A^{3.1}$ in our calculations, close to the M_A^3 theoretical relation.

We also studied the dependence of superdiffusion on the mean free path $\lambda_\parallel$ of the particles. The 3D trajectories of the particles in the MHD turbulence data are presented in Figure 10. Three beams are launched from three randomly selected positions. The (red) beam with a larger mean free path ($\lambda_\parallel \simeq 15L$) exhibits superdiffusion guided by magnetic field lines. In contrast to a hydrodynamic system, the spread is substantially smaller, consistent with an earlier study (Eyink et al. 2013). On the other hand, the (green) beam launched with mean free path $\lambda_\parallel \simeq 0.9L$ displays more stochasticity, in line with the diffusion/random walk process. The blue beam has an intermediate mean free path ($\lambda_\parallel \simeq 1.5L$) and shows characteristics in-between. Figure 11 displays the diffusion index α of CRs as a function of the mean free path $\lambda_\parallel$ in the *local* reference frame. As we see there, the index is dictated by the ratio of $\lambda_\parallel$ to the injection scale L. It changes smoothly from 0.5 according to the normal diffusion regime in the case of $\lambda_\parallel/L \ll 1$ to 1.5 when $\lambda_\parallel/L \gg 1$ in correspondence to Richardson diffusion. In particular, superdiffusion becomes 0.75 when $\lambda_\parallel \sim L$.

6. Discussion

Cosmic ray transport is intimately linked to the properties of MHD turbulence. Different from hydrodynamic turbulence, MHD turbulence is much widely diversified depending on the parameters in the local interstellar environment, such as the Mach number and plasma β. Another factor that has been frequently overlooked is the modes composition of MHD turbulence. It can vary substantially depending on the driving mechanism of turbulence (Makwana & Yan 2020). This is particularly important in view of the fact that different MHD modes contribute to CR transport differently. It is therefore inadequate to depict CR transport as that described by Kolmogorov turbulence with one characterization even in the high-energy regime where external turbulence dominates CR scattering.

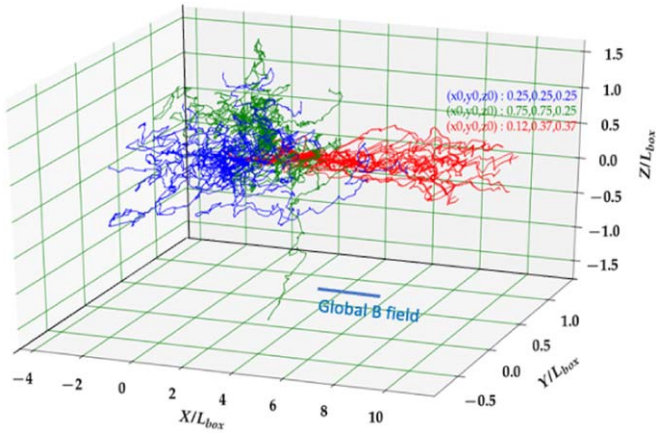

Figure 10. 3D trajectories of particles launched from a beam. They experience superdiffusion because of Richardson diffusion of magnetic fields in turbulence. The rate of superdiffusivity, the α index, depends on the ratio of the mean free path to the injection scale. See also Figure 11.

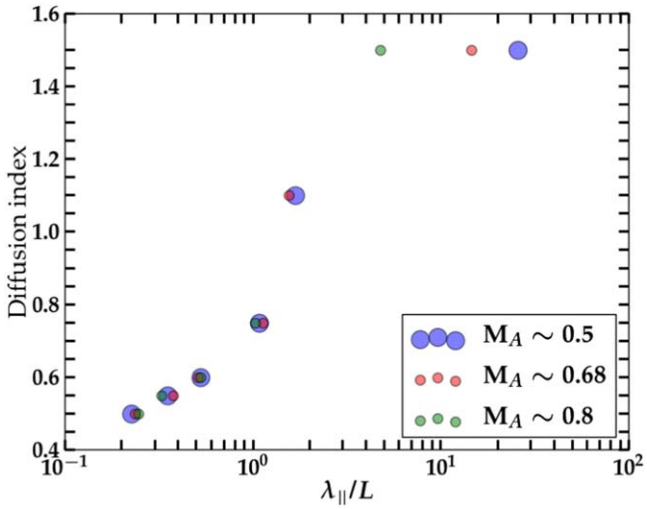

Figure 11. The diffusion index α vs. $\lambda_\parallel$ in the *local* reference frame.

The pitch-angle scattering and therefore parallel diffusion is dominated by fast modes, as confirmed by our test particle simulations here. The parallel diffusion coefficient varies, thereby, with the percentage of fast modes and the forcing mechanism of the local turbulence (Zhang et al. 2020). On the other hand, the cross field transport is much determined by Alfvén modes. As demonstrated in the paper, the tests performed with Alfvén modes show better consistency with theoretical predictions earlier (Yan & Lazarian 2008; Lazarian & Yan 2014) particularly in the *local* reference frame. Then depending on the degree of Alfvénicity (the proportion of Alfvén modes in local MHD turbulence), the observed cross field transport property can vary. The superdiffusion can deviate from the Richardson diffusion determined by the Alfvénicity and the mean free path of the particles. This explains the observed diversity of superdiffusion indices (see, e.g., Perri et al. 2016). The specific M_A dependence can also show some deviation from the theoretical values, e.g., M_A^4 in the case of sub-Alfvénic turbulence and M_A^3 for the super-Alfvénic turbulence.

Damping also plays an important role in shaping the CR diffusion properties, especially the energy dependence. It is, nonetheless, not covered in the test particle simulations with

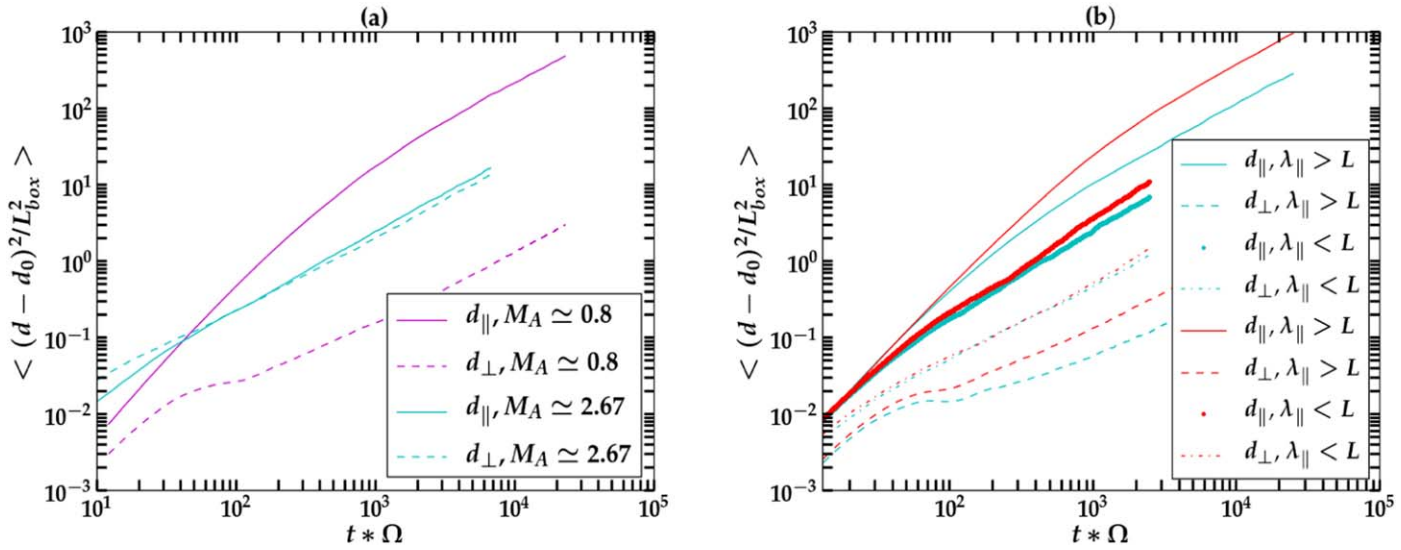

Figure A1. (a) Mean square distance traveled by the particles vs. time. Both sub-Alfvénic ($M_A \simeq 0.8$, magenta) and super-Alfvénic ($M_A \simeq 2.67$, cyan) turbulence are presented. The y-axis represents the mean square distance $< (d - d_0) >^2$ of CR transport normalized by the box length, $L^2_{\rm box}$. The particle running is in the $\lambda_\parallel > L$ regime. The x-axis represents the gyroperiods $t^*\Omega$. The parallel and perpendicular distances obtained from numerical simulations are represented by the bold and dashed lines, respectively. The particles have shown normal diffusion. The diffusion becomes isotropic in the super-Alfvénic turbulence. (b) Same for both CRs with $\lambda_\parallel > L$ and with $\lambda_\parallel < L$ in total turbulence data (green) and Alfvén modes (red) with $M_A \simeq 0.73$. After introducing artificial scattering, the transport becomes more isotropic compared to no artificial scattering.

MHD turbulence because damping physics, collisionless damping in particular, cannot be captured in MHD. We, therefore, do not pay particular attention to the energy dependence of the transport properties. It will be the subject of future studies.

7. Summary

In this paper, we have carried out test particle simulations to study the diffusion of CRs in different MHD turbulence conditions. The particles are considered to have a mean free path $\lambda_\parallel$ both larger and smaller than the injection scale L. The MHD turbulence data cubes range from sub-Alfvénic to super-Alfvénic regimes. The test particle simulations are also performed in the three MHD modes (Alfvén, slow, and fast), decomposed from the MHD turbulence data cubes. The CRs propagating within and beyond the inertial range are investigated. The test particle results are examined in both the local and global reference frames. Our main results are summarized below.

1. The pitch angle scattering test of CRs for different MHD modes shows that: while the pitch angel scattering in Alfvén and slow modes show similar diffusion coefficients, the fast modes differ and are much more efficient in CR scattering.
2. Cross field transport of particles is normal diffusion on large scales. The ratio between the perpendicular and parallel diffusion coefficients is close to the M_A^4 dependence.
3. Particles undergo superdiffusion on scales smaller than the injection scale of turbulence. The superdiffusion rate $d_\perp^2/t^3$ has shown a strong dependence on the Alfvénic Mach number.
4. Richardson superdiffusion is well recovered (1.5 for $\lambda_\parallel > L$) and reduces with the decrease in $\lambda_\parallel$. In particular, the diffusion index becomes 0.75 for $\lambda_\parallel \sim L$, and normal diffusion is recovered when $\lambda_\parallel \ll L$ in the *local* magnetic reference frame with Alfvén modes decomposed from simulated turbulence data. The actual observed diffusion index also varies with the modes composition.

The work is supported by the base funding from DESY. The authors thank the anonymous referee for their valuable comments, which has helped improve the quality of the paper. We acknowledge helpful communications with S. Malik.

Appendix
Diffusion Coefficient for CR Transport on Global Scales

In this section, we present our calculations for the diffusion of CRs on large scales beyond the inertial range. Figure A1(a) demonstrates the parallel and perpendicular distances for CR propagation in sub-/super-Alfvénic turbulence. Figure A1(b) compares the ensemble-averaged square distance of the particles when the mean free path is greater or smaller than the injection scale. In this regime, all our simulations have made sure that the running time is sufficient, and normal diffusion is observed. To perform parallel and perpendicular diffusion coefficients, we take the range when the linear growth is observed in the time evolution figure. We note that in Figure A1(a), the parallel diffusion is much larger than the perpendicular diffusion for $M_A \simeq 0.8$, but they are equal to each other for $M_A \simeq 2.67$. This difference demonstrates the anisotropy is presented in sub-Alfvénic turbulence, but super-Alfvénic turbulence is almost isotropic.

ORCID iDs

Snehanshu Maiti https://orcid.org/0000-0002-0786-7307
Heshou Zhang https://orcid.org/0000-0003-2840-6152
Huirong Yan https://orcid.org/0000-0003-2560-8066

References

Abeysekara, A. U., Albert, A., Alfaro, R., et al. 2017, Sci, 358, 911
Armstrong, J. W., Rickett, B. J., & Spangler, S. R. 1995, ApJ, 443, 209

Beresnyak, A., Yan, H., & Lazarian, A. 2011, ApJ, 728, 60
Chepurnov, A., & Lazarian, A. 2010, ApJ, 710, 853
Cho, J., & Lazarian, A. 2002, PhRvL, 88, 245001
Cho, J., & Lazarian, A. 2003, MNRAS, 345, 325
Earl, J. A. 1974, ApJ, 193, 231
Eyink, G., Vishniac, E., Lalescu, C., et al. 2013, Natur, 497, 466
Goldreich, P., & Sridhar, S. 1995, ApJ, 438, 763
Hentschel, H. G. E., & Procaccia, I. 1984, PhRvA, 29, 1461
Kóta, J., & Jokipii, J. R. 2000, ApJ, 531, 1067
Lazarian, A., Vishniac, E. T., & Cho, J. 2004, ApJ, 603, 180
Lazarian, A., & Yan, H. 2014, ApJ, 784, 38
Lithwick, Y., & Goldreich, P. 2001, ApJ, 562, 279
Liu, R.-Y., Yan, H., & Zhang, H. 2019, PhRvL, 123, 221103
Makwana, K. D., & Yan, H. 2020, PhRvX, 10, 031021
Maron, J., Chandran, B. D., & Blackman, E. 2004, PhRvL, 92, 045001
Perri, S., Amato, E., & Zimbardo, G. 2016, A&A, 596, A34
Perri, S., & Zimbardo, G. 2009, ApJL, 693, L118
Press, W. H., Flannery, B. P., & Teukolsky, S. A. 1986, The Art of Scientific Computing (Cambridge: Cambridge Univ. Press)
Richardson, L. F. 1926, RSPSA, 110, 709
Schlickeiser, R. 2002, Cosmic Ray Astrophysics (Berlin: Springer)
Xu, S., & Yan, H. 2013, ApJ, 779, 140
Yan, H., & Lazarian, A. 2002, PhRvL, 89, 281102
Yan, H., & Lazarian, A. 2004, ApJ, 614, 757
Yan, H., & Lazarian, A. 2008, ApJ, 673, 942
Yan, H., Lazarian, A., & Petrosian, V. 2008, ApJ, 684, 1461
Zhang, H., Chepurnov, A., Yan, H., et al. 2020, NatAs, 4, 1001